

Fusion of Evidences in Intensities Channels for Edge Detection in PolSAR Images

Anderson A. de Borba, Maurício Marengoni, and Alejandro C. Frery, *Senior Member, IEEE*

Abstract—Polarimetric Synthetic Aperture Radar (PolSAR) sensors have reached an essential position in remote sensing. The images they provide have speckle noise, making their processing and analysis challenging tasks. We discuss an edge detection method based on the fusion of evidences obtained in the intensity channels (hh), (hv), and (vv) of PolSAR multi-look images. The method consists of detecting transition points in the thinnest possible range of data that covers two regions using maximum likelihood under the Wishart distribution. The fusion methods used are simple average, multi-resolution discrete (MR-DWT) and stationary (MR-SWT) wavelet transforms, principal component analysis (PCA), ROC statistics, and a multi-resolution method based on singular value decomposition (MR-SVD). A quantitative analysis suggests that MR-SWT provides the best results.

Index Terms—PolSAR, edge detection, maximum likelihood estimation, fusion methods.

I. INTRODUCTION

POLARIMETRIC synthetic aperture radar (PolSAR) has achieved an essential position in remote sensing. The data such sensors provide require specifically tailored signal processing techniques. Among such techniques, edge detection is one of the most important operations for extracting information. Edges are at a higher level of abstraction than mere data and, as such, provide relevant insights about the scene.

Among the available edge detection techniques for SAR and PolSAR images, it is worth mentioning: techniques based on denoising [1]–[5]; Markov random fields [6]; the deep learning approach [7], [8] applied to segmentation and classification; and statistical techniques [9]–[11] applied in edge detection in PolSAR and SAR imagery.

This article follows the statistical modeling approach using the techniques described in [9]–[11] to find edge evidences, followed by fusion processes [12], [13]. Our approach does not attempt to reduce the speckle, but to extract information from its statistical properties.

Instead of handling fully polarimetric data, we treat each intensity channel separately, obtain evidence of edges, and then produce a single estimator of the edge position. With this, we quantify the contribution each channel provides to the solution of the problem.

A. A. de Borba is with the Dept. Engenharia Elétrica e Computação, Universidade Presbiteriana Mackenzie (UPM), and with IBMEC-SP, São Paulo, Brazil. anderson.borba@ibmec.edu.br

M. Marengoni is with the Dept. Engenharia Elétrica e Computação, UPM, São Paulo, Brazil. mauricio.marengoni@mackenzie.br

A. C. Frery is with the Laboratório de Computação Científica e Análise Numérica (LaCCAN), Universidade Federal de Alagoas (UFAL), Maceió, Brazil. acfrery@laccan.ufal.br

The Gambini Algorithm [14] is an attractive edge detection technique. It is local, as it finds evidence of an edge over a thin strip of data; it works with any model, which makes it suitable for SAR data; and it has shown better performance than other approaches. This algorithm consists in casting rays, and then finding the evidence of an edge in the ray by maximizing a value function. The value function we use is the likelihood of two samples: one inside the edge, another outside the edge. Without loss of generality, we assume the complex scaled Wishart distribution for the fully polarimetric observations, from which Gamma laws stem for each intensity channel. The value function depends on the estimates that index such Gamma laws; and we estimate them by maximum likelihood.

The value function is the total likelihood. It is non-differentiable at most points, and classical methods have difficulties in finding the maximum of a non-differentiable functions. We used the Generalized Simulated Annealing (GenSA) [15] method to solve this problem.

We discuss and compare six fusion methods: Simple average [12], Multi-Resolution Discrete Wavelet, MR-DWT [16], Principal Component Analysis, PCA [12], [16], ROC statistics [17], Multi-Resolution Stationary Wavelet Transform, MR-SWT [16], [18], and Multi-Resolution Singular Value Decomposition, MR-SVD [19].

The article is structured as follows. Section II describes statistical modeling. Section III describes edge detection for PolSAR data. Section IV describes the approach to edge evidence fusing. Section V presents numerical results. Finally, Section VI concludes the work with observations, future directions of research, and the feasibility of detecting edges in each channel of PolSAR images.

II. STATISTICAL MODELING FOR POLSAR DATA

Multi-looked fully polarimetric data follow the Wishart distribution with PDF defined by:

$$f_{\mathbf{Z}}(\mathbf{Z}; \boldsymbol{\Sigma}, L) = \frac{L^{mL} |\mathbf{Z}|^{L-m}}{|\boldsymbol{\Sigma}|^L \Gamma_m(L)} \exp(-L \text{tr}(\boldsymbol{\Sigma}^{-1} \mathbf{Z})), \quad (1)$$

where, L is the number of looks, $\text{tr}(\cdot)$ is the trace operator of a matrix, $\Gamma_m(L)$ is the multivariate Gamma function defined by $\Gamma_m(L) = \pi^{\frac{1}{2}m(m-1)} \prod_{i=0}^{m-1} \Gamma(L-i)$, and $\Gamma(\cdot)$ is the Gamma function. We used three $m = 3$ channels in this study. This situation is denoted by $\mathbf{Z} \sim W(\boldsymbol{\Sigma}, L)$, which satisfies $E[\mathbf{Z}] = \boldsymbol{\Sigma}$. This assumption usually holds for fully developed speckle but, since we will estimate L locally instead of considering the same number of looks for the whole image, we will in part take into account departures from such hypothesis.

Fully polarimetric data may be modeled by (1). Since we are interested in describing the information conveyed by parts of such matrix, we rely on the results presented in [20]. In particular, we assume that the distribution of each intensity channel is a Gamma law with probability density function

$$f_Z(z; \mu, L) = \frac{L^L z^{L-1}}{\mu^L \Gamma(L)} \exp\{-Lz/\mu\}, \quad z > 0, \quad (2)$$

where $L > 0$ (rather than $L \geq 1$ to allow for flexibility), and $\mu > 0$ is the mean. The reduced log-likelihood of the sample $\mathbf{z} = (z_1, \dots, z_n)$ under this model is

$$\mathcal{L}(L, \mu; \mathbf{z}) = n[L \ln(L/\mu) - \ln \Gamma(L)] + L \sum_{k=1}^n \ln z_k - \frac{L}{\mu} \sum_{k=1}^n z_k. \quad (3)$$

We obtain $(\hat{L}, \hat{\mu})$, the maximum likelihood estimator (MLE) of (L, μ) based on \mathbf{z} , by maximizing (3) with the BFGS method [21]. We prefer optimization to solving $\nabla \ell = \mathbf{0}$ for improved numerical stability.

III. EDGE DETECTION ON A SINGLE DATA STRIP

The Gambini algorithm estimates the point at which the properties of a sample change. It has been used with stochastic distances [11], and with the likelihood function [9], [10] for edge detection in SAR/PolSAR imagery. It can be adapted to any suitable measure of dissimilarity between two samples.

The algorithm starts by casting rays from a point inside the candidate region, e.g., the centroid. Data are collected around each ray to form the sample $\mathbf{z} = (z_1, z_2, \dots, z_n)$, which is partitioned at position j :

$$\mathbf{z} = (\underbrace{z_1, z_2, \dots, z_j}_{\mathbf{z}_I}, \underbrace{z_{j+1}, z_{j+2}, \dots, z_n}_{\mathbf{z}_E}).$$

We assume two (possibly) different models for each partition: $\mathbf{Z}_I \sim \Gamma(\mu_I, L_I)$, and $\mathbf{Z}_E \sim \Gamma(\mu_E, L_E)$. We then estimate (μ_I, L_I) and (μ_E, L_E) with \mathbf{z}_I and \mathbf{z}_E , respectively, by maximizing (3), and obtain $(\hat{\mu}_I, \hat{L}_I)$ and $(\hat{\mu}_E, \hat{L}_E)$.

We then compute the reduced log-likelihood of \mathbf{z}_I and \mathbf{z}_E :

$$\begin{aligned} \mathcal{L}(j; \hat{\mu}_I, \hat{L}_I, \hat{\mu}_E, \hat{L}_E) = & j[\hat{L}_I \ln(\hat{L}_I/\hat{\mu}_I) - \ln \Gamma(\hat{L}_I)] + \hat{L}_I \sum_{k=1}^j \ln z_k - \frac{\hat{L}_I}{\hat{\mu}_I} \sum_{k=1}^j z_k + \\ & (n-j)[\hat{L}_E \ln(\hat{L}_E/\hat{\mu}_E) - \ln \Gamma(\hat{L}_E)] + \hat{L}_E \sum_{k=j+1}^n \ln z_k - \\ & \frac{\hat{L}_E}{\hat{\mu}_E} \sum_{k=j+1}^n z_k, \end{aligned} \quad (4)$$

and the estimate of the edge position on the ray is the coordinate \hat{j} which maximizes it.

Algorithm 1 is the pseudocode of the basic edge detection with the Gambini Algorithm. We found that one hundred rays is a good compromise between spatial continuity and computational load. Also, \min_s is the minimum sample size that we set to 14.

In our implementation, we replace the exhaustive sequential search (the innermost **for** loop) by Generalized Simulated Annealing (GenSA [15]).

Data: n_c intensity bands, centroid, number of rays

Result: n_c binary images with evidences of edges

for each band $1 \leq c \leq n_c$ **do**

for each ray passing through the centroid **do**
 $\mathbf{z} = (z_1, z_2, \dots, z_n) \leftarrow$ data collected around
 the ray with the Bresenham's midpoint line
 algorithm;

for each $\min_s \leq j \leq n - \min_s$ **do**
 Partition the sample as $\mathbf{z}_I = (z_{\min_s}, \dots, z_j)$
 and $\mathbf{z}_E = (z_{j+1}, \dots, z_{n-\min_s})$;
 Compute $(\hat{\mu}_I, \hat{L}_I)$ with \mathbf{z}_I , and $(\hat{\mu}_E, \hat{L}_E)$
 with \mathbf{z}_E ;
 Compute the total log-likelihood at j as
 $\mathcal{L}(j; \hat{\mu}_I, \hat{L}_I, \hat{\mu}_E, \hat{L}_E)$;

end

$\hat{j} \leftarrow$ the value of j at which the log-likelihood
 function is maximized;

return (\hat{x}, \hat{y}) , the coordinates of each \hat{j} ;

end

return the binary image $\hat{\mathbf{J}}_c$ with 1 at every (\hat{x}, \hat{y}) ,
 and 0 otherwise.

end

Algorithm 1: Gambini algorithm for intensity channels

IV. FUSION OF EVIDENCES

Assume we have n_c binary images $\{\hat{\mathbf{J}}_c\}_{1 \leq c \leq n_c}$ in which 1 denotes an estimate of edge and 0 otherwise. They have common size $m \times n$; denote $\ell = mn$. These images will be fused to obtain the binary image \mathbf{J}_F .

We compare the results of six fusion techniques, namely: simple average, multi-resolution discrete wavelet transform (MR-DWT), principal components analysis (PCA), ROC statistics, multi-resolution stationary wavelet transform (MR-SWT), and multi-resolution singular value decomposition (MR-SVD).

A. Simple Average

The simple average fusion method proposes the arithmetic mean of the edge evidence in each of the n_c channels: $\mathbf{J}_F(x, y) = (n_c)^{-1} \sum_{c=1}^{n_c} \hat{\mathbf{J}}_c(x, y)$, where $1 \leq x \leq m$ indexes the rows, and $1 \leq y \leq n$ the columns of the image.

B. Multi-Resolution Discrete Wavelet – MR-DWT

This section is based on [16]. We apply DWT filters on each binary image $\hat{\mathbf{J}}_c$: a low-pass filter \mathbf{L} in the vertical direction, and a high-pass filter \mathbf{H} in the horizontal direction, then both are down-sampled to create the coefficient matrices $\hat{\mathbf{J}}_{cL}$ and $\hat{\mathbf{J}}_{cH}$. These operations are repeated on the coefficient matrices, leading to $\hat{\mathbf{J}}_{cLL}$, $\hat{\mathbf{J}}_{cLH}$, $\hat{\mathbf{J}}_{cHL}$, and $\hat{\mathbf{J}}_{cHH}$.

The DWT fusion method has the following steps:

- 1) Calculate the DWT decomposition $\hat{\mathbf{J}}_{cLL}$, $\hat{\mathbf{J}}_{cLH}$, $\hat{\mathbf{J}}_{cHL}$, and $\hat{\mathbf{J}}_{cHH}$, for each channel.
- 2) Compute $\bar{\mathbf{J}}_{cHH}$, the pixel-wise mean of all $\hat{\mathbf{J}}_{cHH}$ decompositions.
- 3) Find the pixel-wise maximum of $\hat{\mathbf{J}}_{cLL}$, $\hat{\mathbf{J}}_{cLH}$, $\hat{\mathbf{J}}_{cHL}$: $\bar{\mathbf{J}}_{cLL}$, $\bar{\mathbf{J}}_{cLH}$, and $\bar{\mathbf{J}}_{cHL}$.

- 4) The result of the fusion I_F is the inverse DWT transform of the coefficient matrices $\bar{J}_{c\text{HH}}$, $\bar{J}_{c\text{LL}}$, $\bar{J}_{c\text{LH}}$, and $\bar{J}_{c\text{HL}}$.

C. Principal Component Analysis – PCA

This section is based on [12], [16]. The method is comprised of the following steps:

- 1) Stack the binary images \hat{J}_c in column vectors to obtain the matrix $X_{\ell \times n_c}$.
- 2) Calculate the covariance matrix $C_{n_c \times n_c}$ of $X_{\ell \times n_c}$.
- 3) Compute the matrices of eigenvalues (Λ) and eigenvectors (V) of the covariance matrix, sorted in decreasing order by the eigenvalues.
- 4) Compute the vector $P = (\sum_{c=1}^{n_c} V(c))^{-1}V$, where V is eigenvector associated with the highest eigenvalue of $C_{n_c \times n_c}$; notice that $\sum_{c=1}^{n_c} P(c) = 1$.
- 5) Fuse $I_F(x, y) = \sum_{c=1}^{n_c} P(c)\hat{J}_c(x, y)$.

D. ROC Statistics

The ROC method was proposed and described on [17]:

- 1) Add the binary images \hat{J}_c to produce the frequency matrix (V).
- 2) Use thresholds ranging from $t = 1, \dots, n_c$ on V to generate matrices M_t .
- 3) Compare each M_t with all \hat{J}_c , find the confusion matrix to generate the ROC curve. The optimal threshold corresponds to the point of the ROC curve closest (in the sense of the Euclidean distance) to the diagnostic line.
- 4) The fusion I_F is the matrix M_t which corresponds to the optimal threshold.

E. Multi-Resolution Stationary Wavelet Transform – MR-SWT

This section is based on [16], [18]. The difference between MR-DWT and MR-SWT method is the replacement of the method discrete wavelet transform (DWT) by the method stationary wavelet transform SWT.

F. Multi-Resolution Singular Value Decomposition – MR-SVD

MR-SVD Fusion [19] works similarly to MR-DWT. The difference consists in changing the DWT filters by the SVD filters. The MR-SVD fusion method can be summarized as follows:

- 1) Organize the binary image \hat{J}_c as non-overlapping 2×2 blocks, and arrange each block as a 4×1 vector by stacking columns to form the data matrix X_1 with dimension $4 \times \ell/4$.
- 2) Find the SVD decomposition of $X_1 = U_1 S_1 V_1^T$, where U_1 is a 4×4 unitary matrix, S_1 is a $4 \times \ell/4$ rectangular diagonal matrix known as singular values matrix, and V_1 is an $\ell/4 \times \ell/4$ unitary matrix. The singular values are ordered in a decreasing order.
- 3) Transform the lines of $\widehat{X}_1 = U_1^T X_1 = S_1 V_1^T$ into new matrices with dimensions $m/2 \times n/2$: $\{\Phi_1, \Psi_{1V}, \Psi_{1H}, \Psi_{1D}\}$.
- 4) Repeat the procedure (1) on Φ_r by $r = 2$ up to the lowest resolution level R .

- 5) The MR-SVD decomposition in each channel is

$$\widehat{X}_c \rightarrow \{\Phi_R^c, \{\Psi_{rV}^c, \Psi_{rH}^c, \Psi_{rD}^c\}_{r=1}^R, \{U_r^c\}_{r=1}^R\}.$$

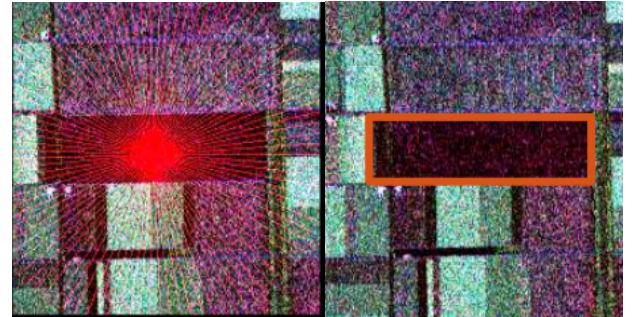
- 6) Once the decomposition is applied to all channels, compute the average of Φ_R^c (Φ_R^f) in the lowest resolution level, and the average of U_r^c (U_r^f), for each r , where f denotes the fusion among channels.
- 7) Find the pixel-wise maxima of Ψ_{rV}^c , Ψ_{rH}^c and Ψ_{rD}^c : Ψ_{rV}^f , Ψ_{rH}^f , Ψ_{rD}^f .
- 8) The fusion I_F is the SVD transformation for each level $r = R, \dots, 1$,

$$I_F \leftarrow \{\Phi_R^f, \{\Psi_{rV}^f, \Psi_{rH}^f, \Psi_{rD}^f\}_{r=R}^1, \{U_r^f\}_{r=R}^1\}.$$

V. RESULTS

A. PolSAR image

We used a 750×1024 pixels AIRSAR PolSAR image of Flevoland, L-band, for the tests. Fig. 12(a) shows the ROI, with the radial lines where edges are detected. Fig. 12(b) shows the ground reference in red.



(a) Image, Region of Interest (ROI), (b) Ground reference and rays.

Fig. 1. Flevoland image in Pauli decomposition, and ground reference

Figs. 2(a), 2(b), and 2(c) show, respectively, the edge evidences in the hh, hv and vv channels as obtained by MLE.

It is worth noting that GenSA has accurately identified the maximum value of ℓ (Eq. (4)), even in the presence of multiple local maxima. A visual assessment leads to conclude that the best results are provided by hv, although with a few points far from the actual edge.

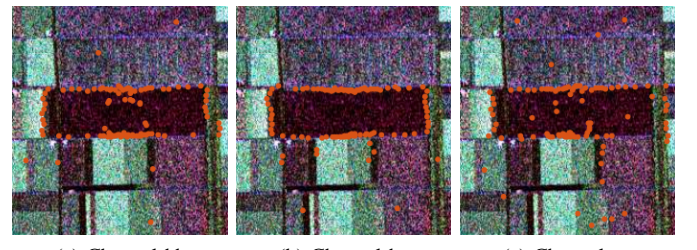


Fig. 2. Edges evidences from the three intensity channels

Figs. 6(a), (b), (c), (d), (e), and (f) show the results of fusing these evidences.

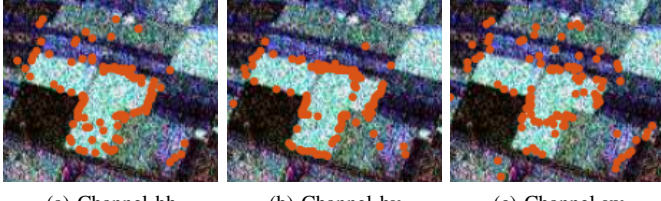


Fig. 3. Edges evidences from the three intensity channels to ROI II - cuidado

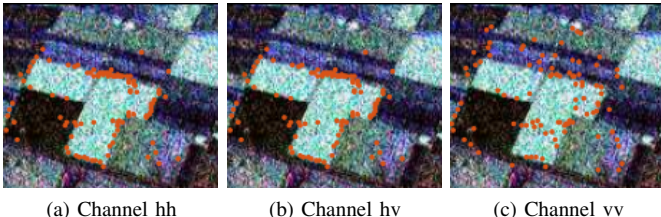


Fig. 4. Edges evidences from the three intensity channels to ROI II - cuidado 2

The simple average and PCA produce similar results. MR-SVD produces considerably less outliers than the other methods, at the cost of longer processing time. ROC produces accurate edges, with few outliers, but sparsely. Both wavelet-based methods (DWT and SWT) produce too dense edges and many outliers.

Figure 19 shows the error of \hat{j} in finding the true edge, as measured on 100 radial lines: the minimum Euclidean distance among the ground truth pixel and the several pixels detected in the fusion methods. We use relative frequencies to estimate the probability of having an error smaller than a number of pixels. Denoting $H(k)$ the number of replications for which the error is less than k pixels, an estimate of this probability is $f(k) = H(k)/n_r$, where n_r is number of radii. In our analysis, k varies between 1 and 10, and $n_r = 100$. The algorithm is described in Ref. [10].

B. Implementation Details

The system presented here was executed on a Intel® Core i7-9750HQ CPU 2.6 GHz 16 GB RAM computer. The method for detecting edge evidence MLE was implemented in the R language. The fusion methods were implemented in Matlab.

Table I shows the running times (absolute and relative to the fastest method).

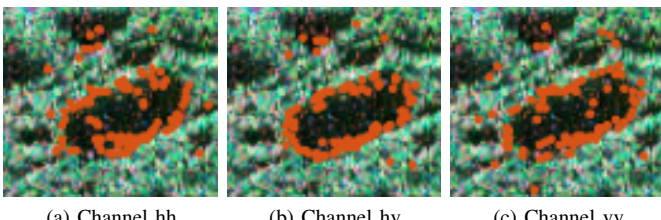


Fig. 5. Edges evidences from the three intensity channels to San Francisco

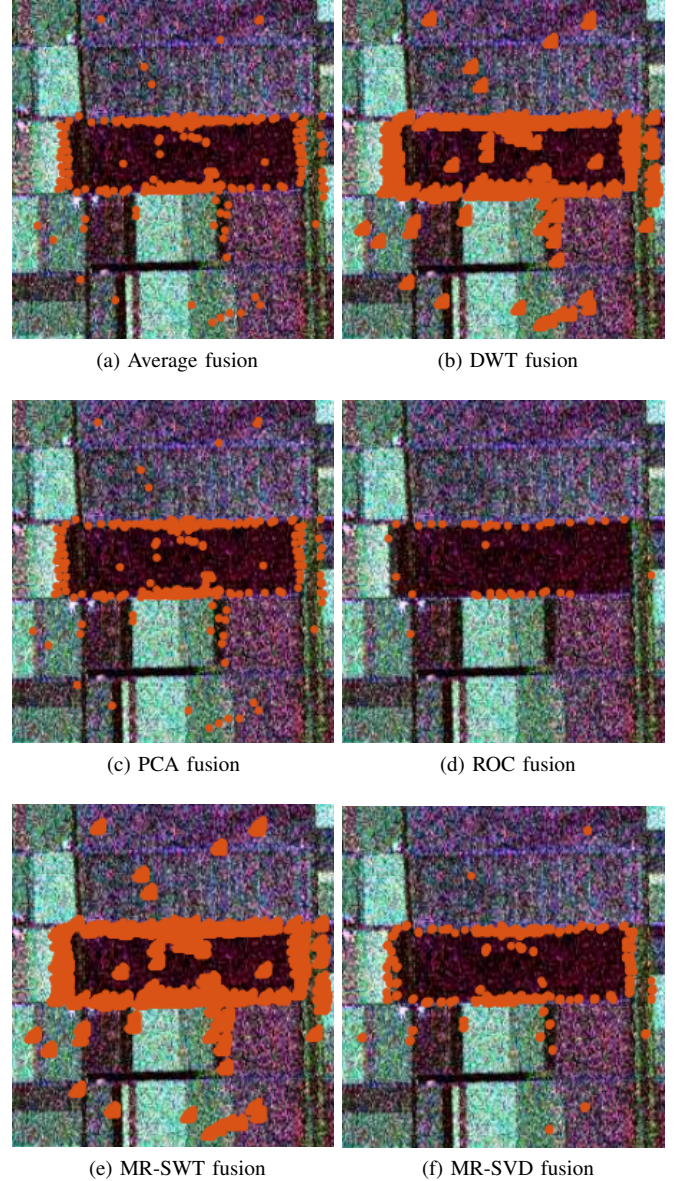


Fig. 6. Results of applying the six fusion methods

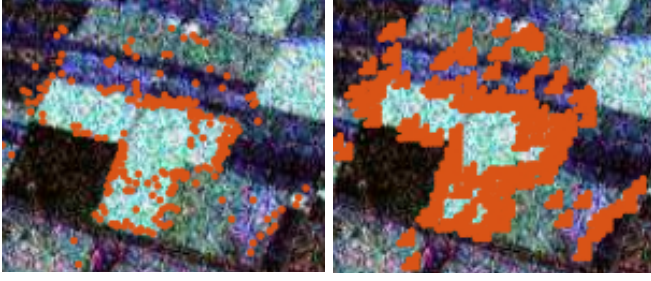
TABLE I
PROCESSING TIMES (FUSION METHOD).

Method	Aver	PCA	MR-DWT	MR-SWT	ROC	MR-SVD
Time (s)	0.01	0.02		0.08		0.18
Rel. time	1.00	2.19		9.25		46.59

VI. CONCLUSION

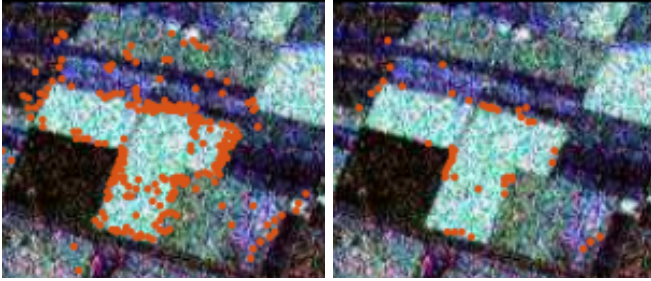
We found evidence of edges using the maximum likelihood method under the Wishart model for PolSAR data. The evidence was found in each of the three intensity channels of an AIRSAR L-band image over Flevoland.

The best edge evidence was observed on the hv channel. We assessed the result by checking the closeness of the fused points to the actual edge, by the presence of outliers, and by the blurring effect.



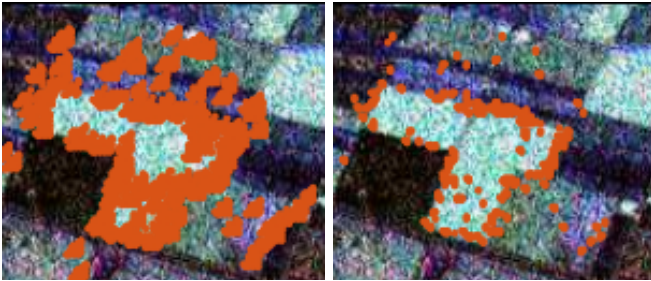
(a) Average fusion

(b) DWT fusion



(c) PCA fusion

(d) ROC fusion



(e) MR-SWT fusion

(f) MR-SVD fusion

Fig. 7. Results of applying the six fusion methods to ROI II

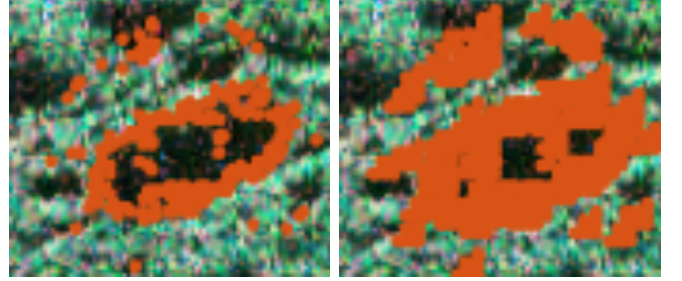
We applied simple average, MR-DWT, PCA, ROC, MR-SWT, and MR-SVD fusion methods to aggregate the evidence obtained in the three channels. The best result was produced by the Multi-Resolution Stationary Wavelet Transform (MR-SWT) with a moderate cost of the processing time.

We highlight two avenues for future improvement of the fusion:

- 1) increasing the number of evidences. This is possible, since fully polarimetric data are richer than mere intensity channels; and
- 2) post-processing of both partial evidences and fusion.

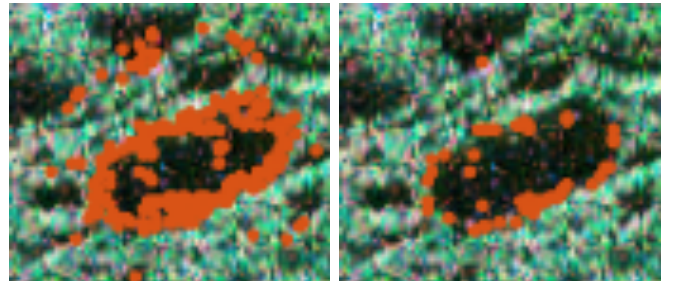
REFERENCES

- [1] J. Shi, H. Jin, and Z. Xiao, “A novel hybrid edge detection method for polarimetric SAR images,” *IEEE Access*, vol. 8, pp. 8974–8991, 2020.
- [2] B. Liu, Z. Zhang, X. Liu, and W. Yu, “Edge extraction for polarimetric SAR images using degenerate filter with weighted maximum likelihood estimation,” *IEEE Geoscience and Remote Sensing Letters*, vol. 11, no. 12, pp. 2140–2144, Dec 2014.
- [3] W. Wang, D. Xiang, Y. Ban, J. Zhang, and J. Wan, “Enhanced edge detection for polarimetric SAR images using a directional span-driven adaptive window,” *Int. J. Remote Sens.*, vol. 39, no. 19, pp. 6340–6357, 2018.
- [4] J. Lee, T. L. Ainsworth, and Y. Wang, “A review of polarimetric SAR speckle filtering,” in *2017 IEEE International Geoscience and Remote Sensing Symposium (IGARSS)*, July 2017, pp. 5303–5306.
- [5] D. Santana-Cedrés, L. Gomez, L. Alvarez, and A. C. Frery, “Despeckling PolSAR images with a structure tensor filter,” *IEEE Geoscience and Remote Sensing Letters*, vol. 17, no. 2, pp. 357–361, Feb 2020.
- [6] F. Baselice and G. Ferraioli, “Statistical edge detection in urban areas exploiting SAR complex data,” *IEEE Geosci. Remote Sens. Lett.*, vol. 9, no. 2, pp. 185–189, March 2012.
- [7] J. E. Ball, D. T. Anderson, and C. S. Chan, “Comprehensive survey of deep learning in remote sensing: theories, tools, and challenges for the community,” *J. Appl. Remote Sens.*, vol. 11, no. 04, p. 1, sep 2017.
- [8] X. X. Zhu, D. Tuia, L. Mou, G. Xia, L. Zhang, F. Xu, and F. Fraundorfer, “Deep learning in remote sensing: A comprehensive review and list of resources,” *IEEE Geosci. Remote Sens. Mag.*, vol. 5, no. 4, pp. 8–36,



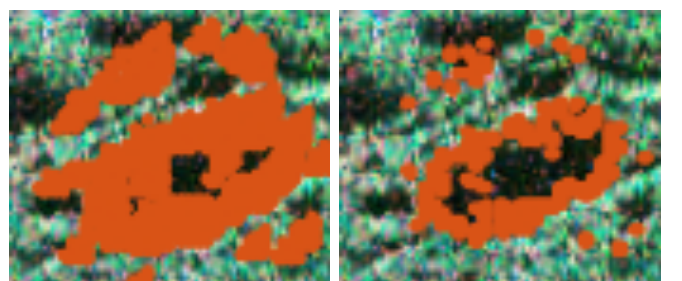
(a) Average fusion

(b) DWT fusion



(c) PCA fusion

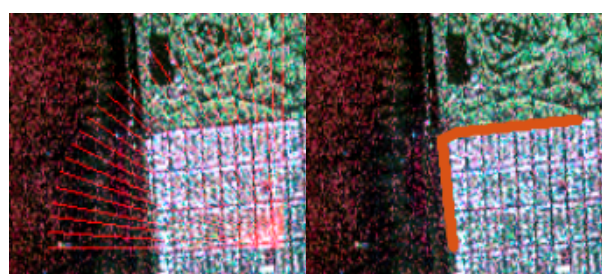
(d) ROC fusion



(e) MR-SWT fusion

(f) MR-SVD fusion

Fig. 8. Results of applying the six fusion methods to San Francisco



(a) Image, Region of Interest (ROI), and rays.

(b) Ground reference

Fig. 9. San francisco image in Pauli decomposition, and ground reference

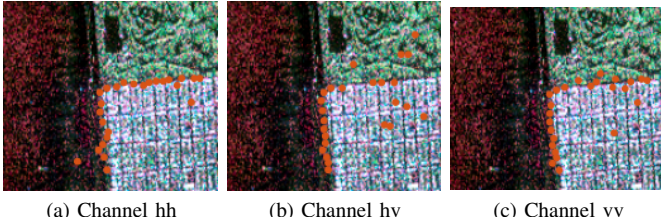


Fig. 10. Edges evidences from the three intensity channels to San Francisco

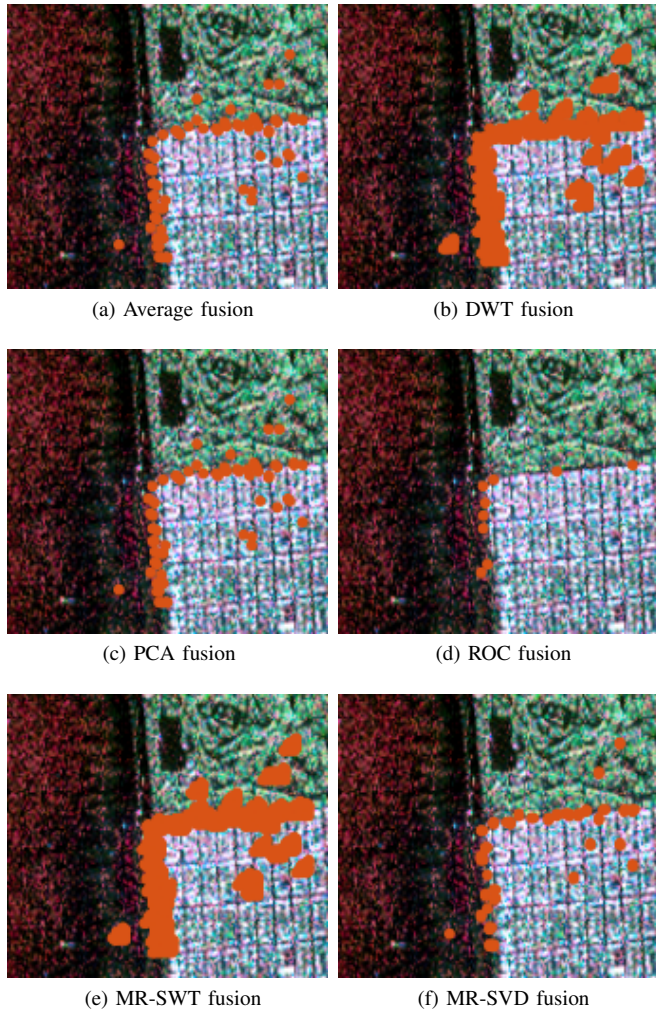


Fig. 11. Results of applying the six fusion methods to San Francisco

- Dec 2017.
- [9] J. Gambini, M. Mejail, J. Jacobo-Berlles, and A. C. Frery, "Feature extraction in speckled imagery using dynamic B-spline deformable contours under the G0 model," *Int. J. Remote Sens.*, vol. 27, no. 22, pp. 5037–5059, 2006.
 - [10] A. C. Frery, J. Jacobo-Berlles, J. Gambini, and M. Mejail, "Polarimetric SAR image segmentation with B-Splines and a new statistical model," *Multidimension. Syst. Signal Process.*, vol. 21, pp. 319–342, 2010.
 - [11] A. Nascimento, M. Horta, A. Frery, and R. Cintra, "Comparing edge detection methods based on stochastic entropies and distances for PolSAR imagery," *IEEE J. Sel. Topics Appl. Earth Observ. Remote Sens.*, vol. 7, no. 2, pp. 648–663, 2014.
 - [12] H. Mitchell, *Image Fusion: Theories, Techniques and Applications*. Springer Berlin Heidelberg, 2010.
 - [13] A. A. de Borba, M. Marengoni, and A. C. Frery, "Fusion of evidences for edge detection in PolSAR images," in *2019 IEEE Recent Advances in Geoscience and Remote Sensing: Technologies, Standards and Applications (TENGARSS)*, Oct 2019, pp. 80–85.

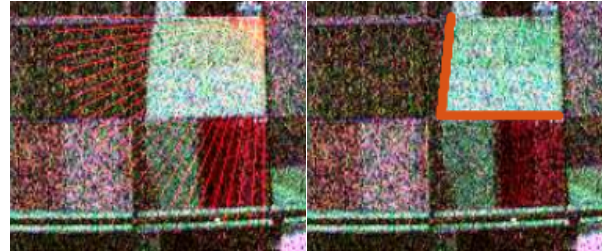


Fig. 12. Flevoland image in Pauli decomposition, and ground reference (ROI), and rays.

(a) Image, Region of Interest (ROI) (b) Ground reference

(c) Pauli decomposition, and ground reference

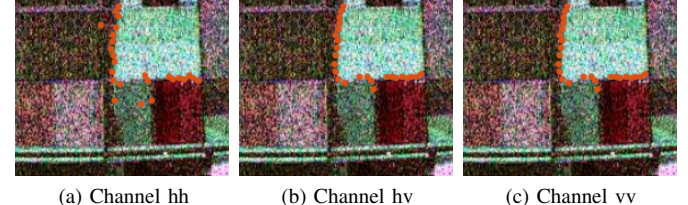
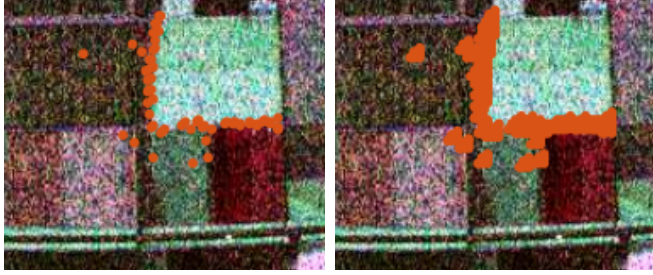


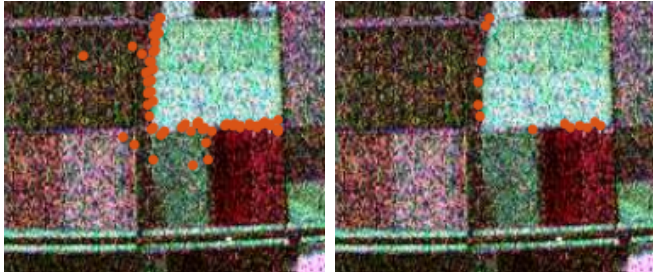
Fig. 13. Edges evidences from the three intensity channels to San Francisco

- in Geoscience and Remote Sensing: Technologies, Standards and Applications (TENGARSS)*, Oct 2019, pp. 80–85.
- [14] J. Gambini, M. Mejail, J. Jacobo-Berlles, and A. C. Frery, "Accuracy of edge detection methods with local information in speckled imagery," *Statistics and Computing*, vol. 18, no. 1, pp. 15–26, 2008.
 - [15] Y. Xiang, S. Gubian, B. Suomela, and J. Hoeng, "Generalized Simulated Annealing for Global Optimization: The GenSA Package," *The R Journal*, vol. 5, no. 1, pp. 13–28, 2013.
 - [16] V. Naidu and J. Raol, "Pixel-level image fusion using wavelets and principal component analysis," *Defence Science Journal*, vol. 58, pp. 338–352, Mar. 2008.
 - [17] S. Giannarou and T. Stathaki, "Optimal edge detection using multiple operators for image understanding," *EURASIP Journal on Advances in Signal Processing*, vol. 2011, no. 1, p. 28, Jul 2011.
 - [18] Q. Jiang, X. Jin, S. Lee, and S. Yao, "A novel multi-focus image fusion method based on stationary wavelet transform and local features of fuzzy sets," *IEEE Access*, vol. 5, pp. 20286–20302, 2017.
 - [19] V. Naidu, "Image fusion technique using multi-resolution singular value decomposition," *Defence Science Journal*, vol. 61, no. 5, pp. 479–484, Sep. 2011.
 - [20] M. Hagedorn, P. Smith, P. Bones, R. Millane, and D. Pairman, "A trivariate chi-squared distribution derived from the complex Wishart distribution," *Journal of Multivariate Analysis*, vol. 97, no. 3, pp. 655–674, 2006.
 - [21] A. Henningsen and O. Toomet, "maxlik: A package for maximum likelihood estimation in R," *Computational Statistics*, vol. 26, no. 3, pp. 443–458, 2011.



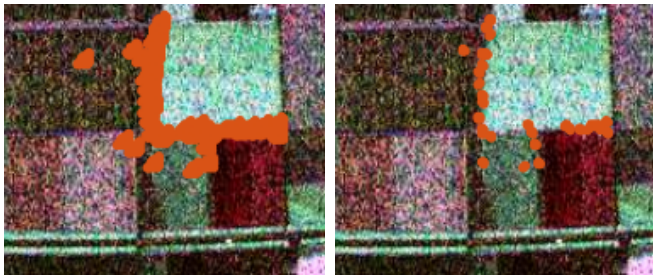
(a) Average fusion

(b) DWT fusion



(c) PCA fusion

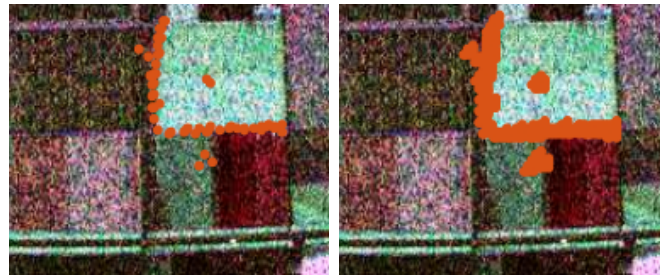
(d) ROC fusion



(e) MR-SWT fusion

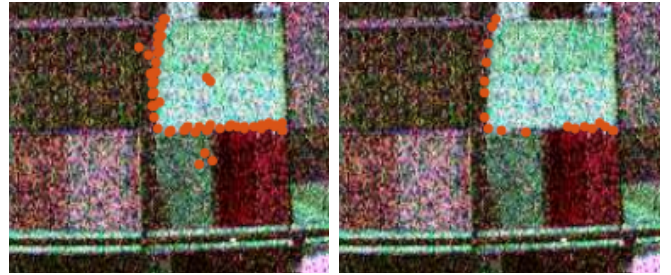
(f) MR-SVD fusion

Fig. 14. Results of applying the six fusion methods to Flevoland III



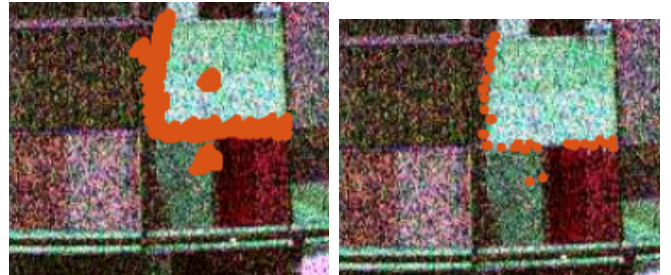
(a) Average fusion

(b) DWT fusion



(c) PCA fusion

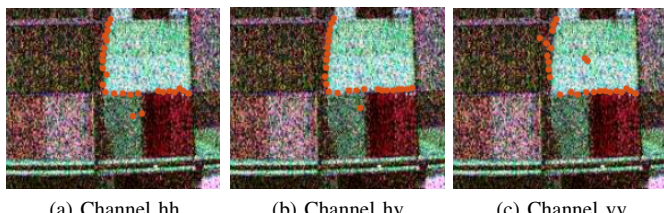
(d) ROC fusion



(e) MR-SWT fusion

(f) MR-SVD fusion

Fig. 16. Results of applying the six fusion methods to Flevoland III - folga 25 pixel



(a) Channel hh

(b) Channel hv

(c) Channel vv

Fig. 15. Edges evidences from the three intensity channels to San Francisco - 25 pixel

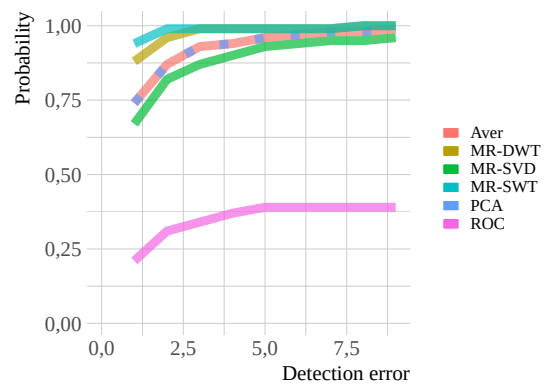


Fig. 17. Probability of detecting in fusion methods.

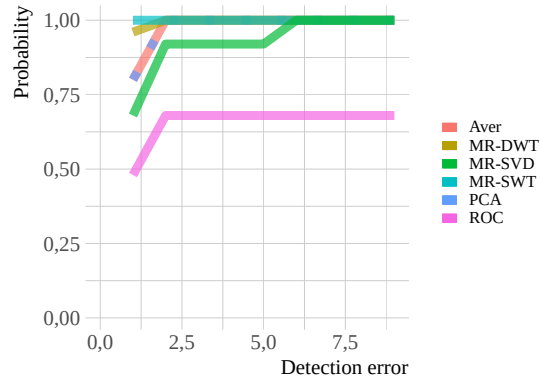


Fig. 18. Probability of detecting in fusion methods. Região III - FLEV

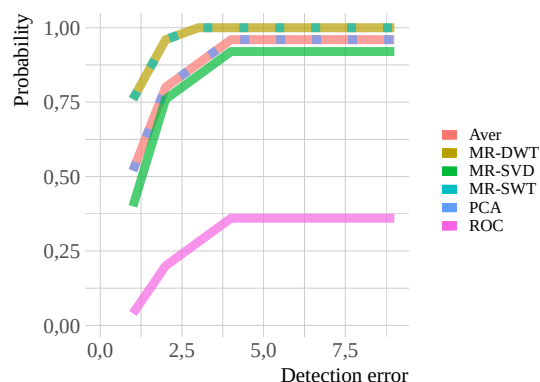


Fig. 19. Probability of detecting in fusion methods. Região I - SF